Article

Ethanol steam reforming on lanthanum Ni-ZrO2 catalysts

Cristina Pizzolitto, Federica Menegazzo, Elena Ghedini, Giada Innocenti, Alessandro Di Michele, Maurizio Mattarelli, Giuseppe Cruciani, Fabrizio Cavani, and Michela Signoretto

ACS Sustainable Chem. Eng., **Just Accepted Manuscript** • DOI: 10.1021/acssuschemeng.0c02373 • Publication Date (Web): 01 Jul 2020

Ethanol steam reforming on lanthanum Ni-ZrO_2 catalysts

*Cristina Pizzolitto,[a] Federica Menegazzo,[a] Elena Ghedini,[a] Giada Innocenti,[b] Alessandro di Michele,[c] Maurizio Mattarelli,[c] Giuseppe Cruciani,[d] Fabrizio Cavani,[b] Michela Signoretto[a]**

a Dr. C. Pizzolitto, Dr. F. Menegazzo, Dr. E. Ghedini, Prof. M. Signoretto, CATMAT Lab, Department of Molecular Sciences and Nanosystems, Ca' Foscari University Venice and INSTM RU of Venice, via Torino 155, I-30172 Venezia Mestre, Italy E-mail: miky@unive.it

b Dr. G. Innocenti, Prof. F. Cavani, Department of Industrial Chemistry "Toso Montanari", University of Bologna, viale Risorgimento 4, I-40136 Bologna, Italy and Consorzio INSTM, UdR di Bologna, Firenze, Italy

c Dr. A. Di Michele, Dr. Maurizio Mattarelli, Department of Physics and Geology, University of Perugia, Via Pascoli 1, I-06123, Perugia, Italy

d Prof. G. Cruciani Department of Physics and Earth Sciences, University of Ferrara, Via Saragat 1, I-44100 Ferrara, Italy

Abstract

Hydrogen is defined the future energy carrier and ethanol steam reforming can be a sustainable process for its production. Promoting addition of lanthanum on Ni-zirconia catalyst was evaluated, with a focus on lanthanum introduction method (incipient wetness impregnation and co-precipitation). Lanthanum addition strongly affected morphological, structural and chemical features of the catalysts. It particularly affected the stabilization of zirconia phase and the surface basic properties. For the promoted materials, higher ethanol conversion and hydrogen yield were obtained. Best catalytic results with the catalyst prepared via promoter impregnation, 81 % of ethanol conversion and 25 % of H_2 yield after 16 hours of reaction were obtained. By CO_2-TPD technique, it was estimated to be the most basic material. DRIFT analyses were used to understand the effect of basic sites in the reaction pathway. High number of medium and strong basic sites reduced the formation of unwanted intermediates such as ethylene. In this way, the formation of coke deposits is reduced. SEM, TG analyses, and Raman spectroscopy confirmed the results.

Keywords: zirconia, lanthanum, ethanol steam reforming, coke deactivation

Introduction

The current worldwide research is focused on finding the most sustainable solution for energy production. In this contest, hydrogen has been considered as one of the most promising answer to overcome the already known drawbacks of fossil sources. This gas, in fact, is an unlimited raw material with a high specific energy density (between 120 MJ/kg to 142 MJ/kg), 2.75 times higher than the other hydrocarbons[1]. It is a clean source, nontoxic and can be used in fuel cell engines to produce electrical energy directly from the chemical one. One of the main problems is that conventional sources dominate its production. Furthermore, to be considered as an environmentally friendly fuel, it must be produced by renewable sources. In this regard, biomass and in particular ethanol, should represent a promising raw material since they can be efficiently converted into hydrogen through steam reforming[2]. Considering ethanol steam reforming (ESR), the efficiency of this process is related to the mole balance: 6 moles of hydrogen can be produced from one mole of ethanol ($CH_3CH_2OH + 3\ H_2O \rightleftarrows 6\ H_2 + 3\ CO_2$) in an endothermic process. Coke production is the main drawback of this reaction. Ethanol, in fact, can follow two main reaction ways; ethanol dehydration to ethylene and ethanol dehydrogenation to acetaldehyde. Both processes are endothermic and can take place in standard reaction conditions (450-750 °C). At the same time, unsaturated hydrocarbons can be polymerized and produce carbon deposits[3].

1) $CH_2{=}CH_2 \rightarrow$ coke

Apart from that, two other reactions can be involved in coke formation:

2) $2\ CO \rightleftarrows CO_2 + C$

3) $CH_4 \rightleftarrows C + 2\ H_2$

Reactions 1) and 2) are predominant at low temperature, as reported by S. Liu *et al.*[4], meanwhile, at high temperature decomposition of methane is the primary source of carbon formation since its decomposition occurs above 900 °C[5]. For all these reasons, a rigorous choice of the catalyst is required[6]. The efficient catalyst must be chosen to maximize H_2 production. In this work, the attention was focused on catalyst formulation. In particular, the role of support in the nickel active phase stabilization was evaluated. The choice of nickel as metal is a good compromise between cost and efficiency. Indeed, it is the traditional active phase used for methane steam reforming[7]. The primary problems of Ni are sintering and deactivation due to carbon deposition. The support has the role to get over the nickel limits, leading to high stability, activity and resistance for the whole process[8-11]. Zirconia is an attractive support for its acidic, basic, oxidizing and reducing properties[12]. Moreover, it contains high thermal stability and redox properties that are used to

catalyse a wide range of reactions such as hydrogenation of olefins, isomerization of olefins and epoxides, and dehydration of alcohols[13]. Furthermore, considering the reforming application, it is an optimal support since it can easily adsorb and dissociate H_2O. In this way, steam is more easily adsorbed on the surface and hydrocarbons gasification and WGSR (water gas shift reaction) are favoured [14]. Moreover, it strongly interacts with nickel particles, preventing metal mobility over the surface and as consequence, metal sintering[15]. Some of the zirconia limitations in ESR are linked to its acid/base features. As it is reported by Ochoa *et al.*[16], acid sites favour ethanol dehydration to ethylene, while basic sites promote dehydrogenation to acetaldehyde. As previously reported, ethylene can be dehydrogenated to ethane and consequently produce coke, by means of reaction 1). The addition of basic promoters such as alkali and alkali-earth metals should reduce the acidity of support thus preventing from unwanted reactions. Therefore, different researchers emphasised the use of promoters, such as calcium, magnesium and potassium in the activity of acidic supports[17,18]. For instance, Nichele *et al.* reported the effect of CaO on zirconia resulted in reduced Lewis acidity of support and inhibition of coke formation. Besides, CaO produces oxygen vacancy on the support, activating CO_2 and H_2O, thus favouring the gasification of coke[19]. Compagnoni *et al.* compared the promotive effect of CaO, MgO and K_2O and found out that among them, CaO and K_2O led to the highest H_2 yield[20]. Besides the metals alkaline and alkaline earthy, the lanthanide were studied as basic promoters. As it is described by Osorio-Vargas *et al.*, lanthanum oxide addition in nickel-alumina catalyst reduces the selectivity to ethylene decreasing support Lewis acidity[21, 22]. At the same time, lanthanum oxide, compared to other basic materials, can interact with the carbonaceous species deposited on metal, freeing the surface. P. Osorio-Vargas *et al.* reported this effect for Ni/Al_2O_3 catalyst[23]; La_2O_3 react with CO_2 to form lanthanum oxycarbonate species ($La_2O_3 + CO_2 \rightleftarrows La_2O_2CO_3$), that therefore can react with carbon-metal species to produce CO ($C\text{-}Me + La_2O_2CO_3 \rightleftarrows 2\,CO + Me + La_2O_3$). Only few papers report the effect of lanthanum addition on nickel zirconia catalyst for H_2 production by ESR [24, 25]. Indeed, the aim of the present work, unlike previous works, is to study how La doping method can influence morphological and structural properties of the material. Moreover, attention was devoted to the correlation between basic properties, reaction mechanism and coke deposition.

Experimental

Synthesis of supports

10 g of zirconia support (Z) were prepared by precipitation from the proper amount of $ZrOCl_2 8H_2O$ (Sigma Aldrich) using 30 mL of NH_3 5M at pH= 8.5. Then it was treated at 90 °C for 20 hours, ~~. The~~

washed and then dried at 110 °C for 18 hours. Then zirconium hydroxide was air annealed for 3 hours at 550 °C.

La addition by either incipient wetness impregnation (IWI) or coprecipitation with Zr. For La*Zimpr* $La(NO_3)_3*6H_2O$ was added to the calcined zirconia to obtain 6 wt % of La. The material was dried at 110 °C for 18 hours and then calcined again under flowing air at 550 °C for 3 hours.

As for co-precipitated support (La*Zcopr*), $La(NO_3)_3*6H_2O$ was dissolved together with the zirconia precursor.

Synthesis of catalysts

Nickel was introduced by IWI of $Ni(NO_3)_2*6H_2O$ to obtain 8.5 wt% Ni. of nickel on the final material. The material was dried at 110 °C for 18 hours and calcined at 550 °C for 4 hours.

The samples will be referred to as:

NiZ

NiLa*Zimpr* (La_2O_3 added by impregnation)

NiLa*Zcopr* (La_2O_3 added by co-precipitation)

Methods

A Micromeritics ASAP 2000 analyser was used for the determination of surface areas and pore size distributions[26].

Temperature programmed reductions (TPR) were tested according to Pizzolitto *et al.*[26].

Temperature programmed desorption of CO_2 (CO_2-TPD) were performed as in ref [27].

The Ni amount was determined by atomic absorption spectroscopy (AAS)[28], while the La amount by MP-AES (Microwave Plasma Atomic Emission Spectroscopy), using MP-AES 4210 (Agilent).

X-ray powder diffraction (XRD) patterns were recorded as reported in ref [19] .

SEM analyses were recorded using a Field Emission Gun Electron Scanning Microscopy LEO 1525[26]

DRIFTS-MS experiment were performed by a Bruker Vertex 70 provided with a Pike DiffusIR cell attachment. Spectra were recorded on EcoSys-P from European Spectrometry Systems using an MCT detector after 128 scans and 4 cm^{-1} resolution. In a typical experiment, the catalyst was pretreated for 1 h at 500 °C in He. Then, backgrounds were recorded every 50 °C from 25 °C to 500 °C. A mixture of EtOH/H_2O (ratio 1/6 w/w, 0.6 0.6 μL min^{-1}) in He (8 ml/min) was fed heating until 500 °C at 5 °C min^{-1}. A spectrum was collected (using the background at the same temperature) every 50 °C. The catalyst behaviour at 500 °C was evaluated for 60 min in presence of the reactant stream, collecting a spectrum every 2.5 min. Analysation of carbon deposit over the catalytic surface were characterized via SEM and Raman spectroscopy.

The Raman measurements were performed by a home made micro Raman spectrometer. The external optics was based on a CM1 microscope purchased from the JRS Scientific Instruments (Switzerland), mounting a 50X long working distance objective (N.A. = 0.55). The Stokes region of the backscattered VV polarized signal was analyzed by a 600 grooves/mm grating and collected by a cooled CCD detector (Syncerity^{TM} 1024 x 256) for a Raman shift ranging between 100 and 3500 cm^{-1}. The actual spectral resolution was about 3 pixels (~10 cm^{-1}). The excitation was provided a DPSS laser with emission centered at 532 nm. As the excitation is focused on a region sized about 1 μm and in order to avoid thermal effects on the sample, the incident power was kept below 10mW.

Catalytic test

ESR was investigated by a PID reference reactor (Process Integral Development Eng&Tech)[29].The mixture of water and ethanol (molar ratio 6:1) was flowing with 0,02 mL/min and helium (230 ml/min) was used as carrier (W/F ratio = 1,44 g*h/gmol). The selected parameter has been chosen based on previous studies conducted on the effect of W/F on the activity of the same systems. The selected value has proven to be the best in discriminating the properties of different materials, enhancing the deactivation mechanism. Moreover, we have selected at high ratio between H_2O and EtOH, to better simulate the real bioethanol composition. No pre-treatment of catalyst was performed. The typical reaction temperature was 550 °C[26]. Preliminary blank tests have shown the absence of conversion at this temperature. Moreover, preliminary tests have demonstrated that the system works in a strictly kinetic regime.

Results and Discussion

Preliminary characterisations

Lanthanum was introduced in the material by two different synthetic approaches to study not only its doping effects, but also the influence of preparation method on the catalyst's properties. Lanthanum incipient wetness impregnation over zirconia (La*Zimpr*) and lanthanum co-precipitation with zirconia (La*Zcopr*) were investigated. First, N_2 adsorption-desorption analyses were performed to determine their surface area and pore size distribution. This aspect is of crucial importance in heterogeneous catalysis due to the fact that a high surface area has positive effect on catalyst activity, allowing a high metal dispersion[30]. The surface area, the pore volume and the mean pore size of the three zirconia samples are reported in the Table 1. The corresponding isotherms are shown in Figure 1. According with IUPAC classification, the three catalysts exhibit a type IV isotherm containing a H_3 hysteresis loop, typical of mesoporous materials that don't have a well-defined mesoporous structure. In detail, NiZ and NiLa*Zimpr* present almost the same isotherms shape and BJH distribution, meanwhile for NiLa*Zcopr*, the surface area is slightly higher, the pore size distribution is broader, and the hysteresis

shape is wider. Thus, it's possible to suppose that lanthanum added by co-precipitation moderately influence the structural properties of zirconia material. Conversely, in the case of impregnation method, this effect has not been indicated because zirconia structure has already been formed during the first calcination step; only a small decrease in BET surface area value due to the introduction of nickel via impregnation method is observed.

Regarding nickel and lanthanum amount, reported in Table 1 and calculated via atomic adsorption and MP-AES, respectively, it is almost the same for all the sample and it agrees with the nominal amount.

	NiZ	NiLaZ*impr*	NiLaZ*copr*
Surface area	45 ± 3 m^2/g	40 ± 3 m^2/g	55 ± 3 m^2/g
Mean pore size	17 nm	18 nm	15 nm
Pore Volume	0.19 cm^3/g	0.18 cm^3/g	0.22 cm^3/g
Nickel amount	8.5 wt%	8.2 wt%	8.6 wt%
Lanthanum amount	0 wt%	4.0 wt%	4.4 wt%

Table 1: Physical and chemical properties of catalysts.

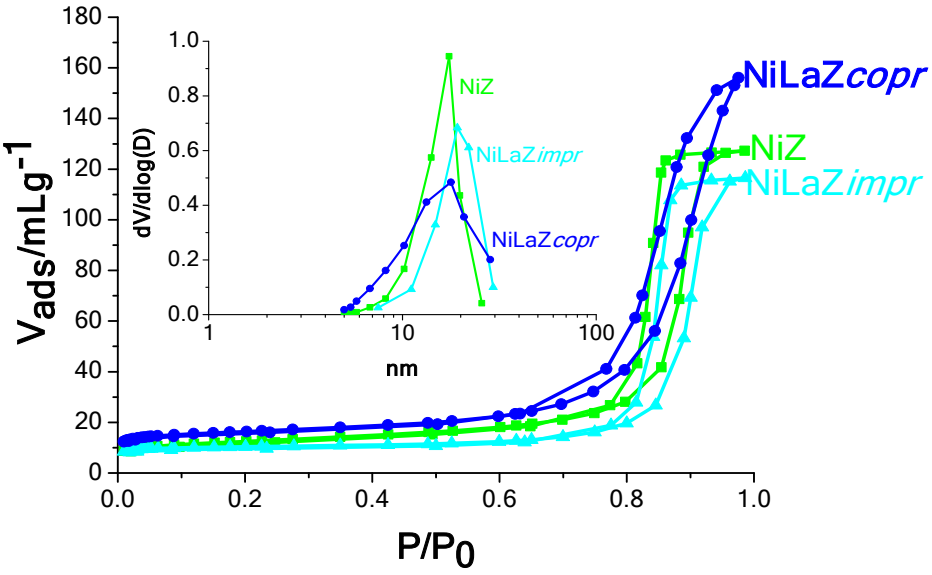

Figure 1: N_2 adsorption/desorption isotherms and BJH curves (inset) of NiZ (■) NiLaZimpr (▲) and NiLaZcopr (●) catalysts

TPR measurements were achieved for the detection of NiO species over the supports according to their reduction temperature (Figure 2). Since nickel presents only one oxidation state transition, from 2+ to 0, and zirconia and lanthanum don't show any reduction peak between 25 °C and 900 °C, the presence of more than one peak suggests different interactions between support and active phase[31-33]. NiZ sample exhibits two different peaks: a small one at 360 °C and a bigger one at 520 °C respectively. The first one is ascribable to nickel lowly interacting with the support and the second one to nickel strongly interplaying with it[34]. In the case of NiLaZ*impr*, these peaks are moved to temperatures of 280 °C and 400 °C, respectively. This result indicates that lanthanum added via impregnation method affects the interactions between nickel and zirconia, reducing their strength and therefore the reduction temperature of the catalyst[35]. In the case of NiLaZ*copr*, the TPR profile is completely different. One broad peak with three different *maxima* is present between 350 °C and 550 °C. This means that there are at least three different NiO species interacting with the support. Moreover, most of the nickel interacts weaker with the support than NiZ since the higher maximum is associated with the peak located at lower temperature. Besides, based on TPR profiles, it's possible to assert that nickel is completely reduced before 550 °C for all the three zirconia catalysts. This is relevant for the ESR reaction conditions that will be discussed later.

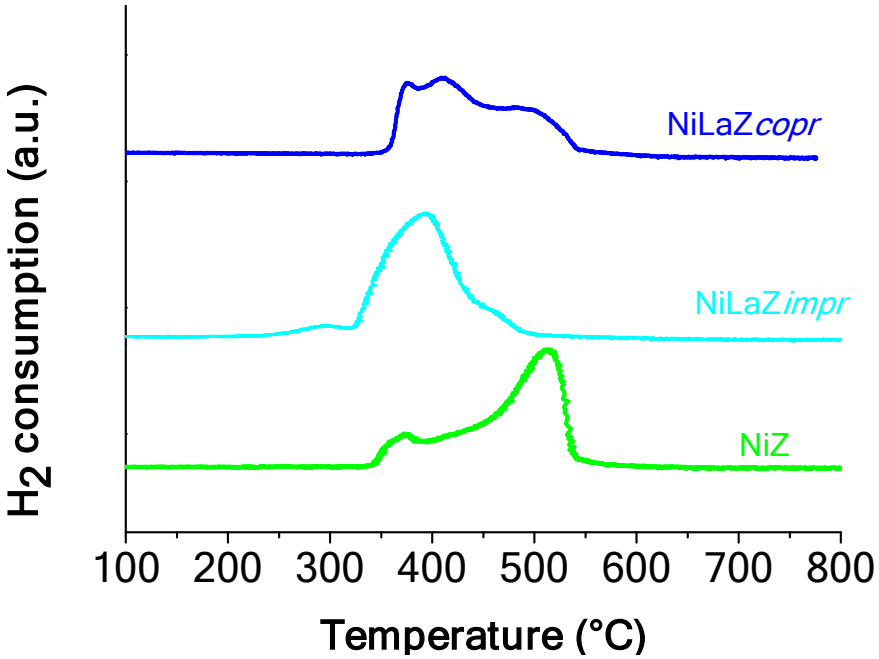

Figure 2: TPR profiles of NiZ, NiLaZ*impr* and NiLaZ*copr* samples.

XRD analyses were performed to identify zirconia polymorph and Ni particle size, using Rietveld refinements. As for the support, looking at Figure 3, it is clear that for NiZ and NiLaZ*impr*, zirconia

is present in two different phases: monoclinic and tetragonal, respectively at 2θ 24.3, 28.0, 31.55, 34.2, 40.8, 44.9, 45.5, 49.4, 54.0, 55.4 ° for monoclinic phase and 2θ 30.2, 35.5 and 50.3 ° for tetragonal phase[36]. La addition caused a slight increase of the tetragonal/monoclinic ratio. By contrast, in the case of NiLaZ*copr,* only tetragonal phase is detected at 2θ 30.2, 35.5 and 50.3 °. Therefore, it seems that lanthanum added on the support via co-precipitation method stabilizes the zirconia tetragonal phase. Tetragonal phase is a zirconia phase that is stable at 1170 °C and it can be kept steady by metal cations incorporation, and this has been widely studied for ceramic applications[37]. For example, the stabilisation of metastable zirconia tetragonal phase with the addition of yttria[38] and with the use of sulfated zirconia[39] have been proven. In this work, we have verified the stabilization of zirconia by lanthanum addition via co-precipitation method. It's important to underline that only with this method it is possible to tune the morphological and structural feature of the material. Therefore, this can be a clear indication that the synthetic approach could strongly affect the final catalysts. In the case of nickel, for all the samples exposed to reduction treatment, it is manifest only in the metallic form (peak at 2θ = 44.5 °). This demonstrates that the step at 550 °C is effective for reducing all Ni^{2+} to Ni^0, according to TPR profiles previously discussed. At the same time, nickel particle size hasn't been affected by lanthanum addition. In particular, the average crystallites size of 13-15 nm has been calculated by Rietveld refinements, respectively NiZ (14 nm), NiLaZ*impr* (13 nm) and NiLaZ*copr* (15 nm). These data agree with SEM results that are shown in Figure 4.

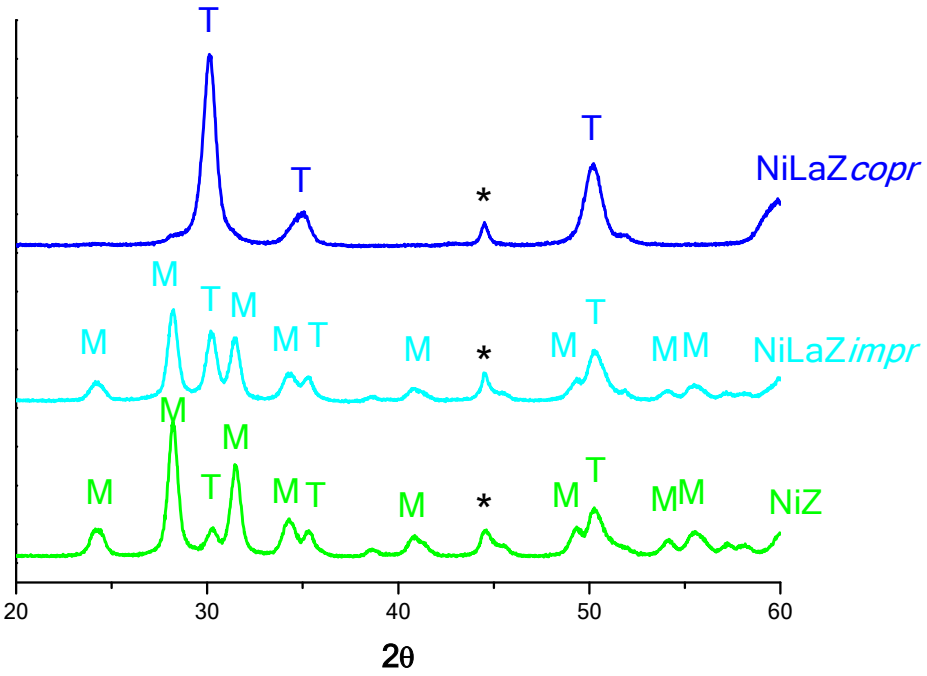

Figure 3: XRD analyses of reduced NiZ, NiLaZ*impr* and NiLaZ*copr* samples (* is the Ni^0 species, M is the zirconia monoclinic phase and T is the zirconia tetragonal phase).

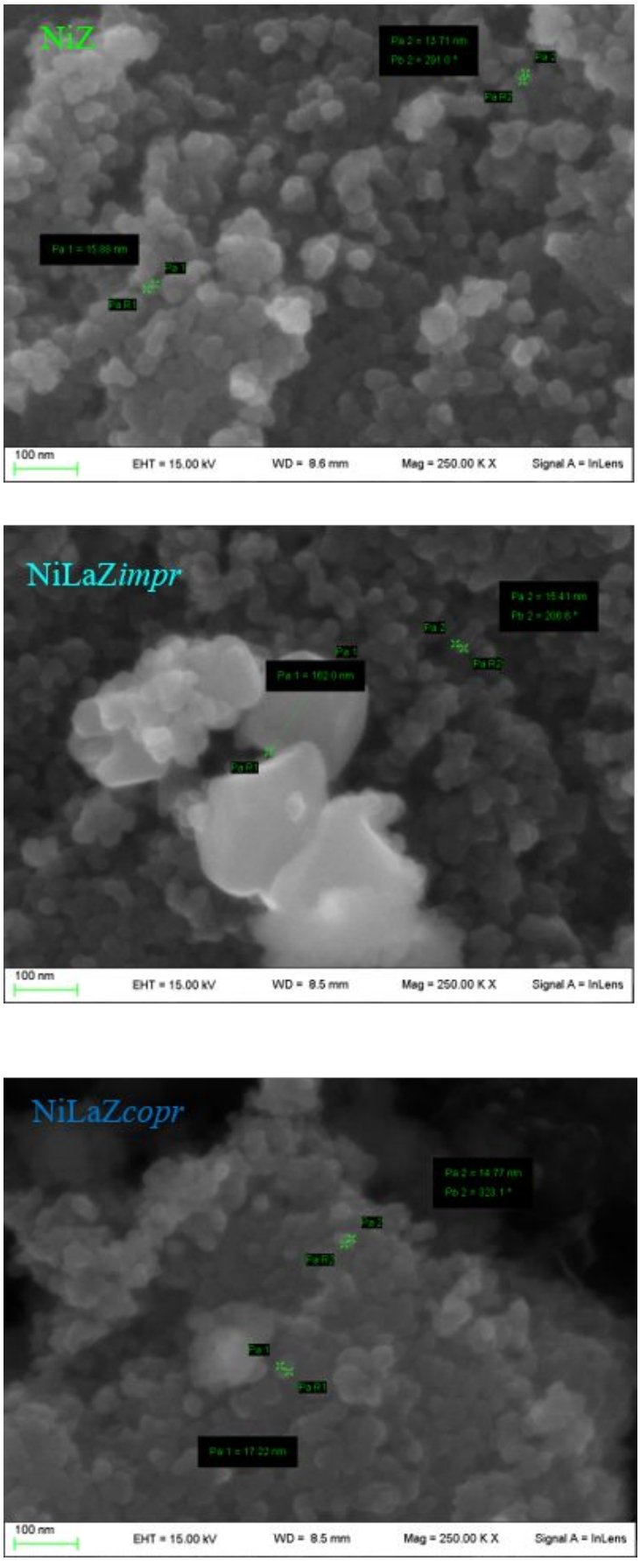

Figure 4: SEM images of as prepared NiZ, NiLaZ*impr* and NiLaZ*copr* samples.

From these preliminary characterizations, it can be concluded that lanthanum added by incipient wetness impregnation (NiLaZ*impr*) doesn't affect the structural and morphological properties of the material, leading similar surface area, pore size distribution and zirconia phases. Only an enhancement of nickel reducibility has been evidenced, even if metal particle size is the same of NiZ catalyst. By contrast, addition of lanthanum by coprecipitation (NiLaZ*copr*) stabilized the tetragonal phase of zirconia, increased the surface area of the support and determined more different nickel species interacting with the support. Therefore, the amount of nickel weakly interacting with the support was increased.

Catalytic tests

These materials were checked in the ESR. Figure 5 shows ethanol conversion vs time of stream, meanwhile in Table 2, H_2 yield and products distribution registered are recorded. As regard as ethanol conversion, a strong promoting effect of lanthanum addition is evident. NiZ sample demonstrates a decrease in ethanol conversion after only two hours of reaction, reaching the value of 44 % on the 16th hour. On the other hand, in the case of both lanthanum promoted samples, ethanol conversion is quite stable till the 4th hour of reaction following with a gradual decrease till 16th hour. Impregnation of lanthanum over calcined zirconia (NiLaZ*impr*) allows to keep 80 % of ethanol conversion, meanwhile for NiLaZ*copr* higher deactivation is visible. The same trends were obtained for hydrogen yield. For NiZ sample, in the first period 50 % of yield is achieved, decreasing to 7 % after 16 hours; meanwhile, for the promoted catalysts, higher H_2 yield is maintained. NiLaZ*copr* gets 15 % of H_2 yield meanwhile NiLaZ*impr* presents the highest activity at the end of the reaction with 25 % of H_2 yield. In the case of products distribution, no differences between the three samples are observed. Carbon monoxide, carbon dioxide and hydrogen are the only depicted products, and their distribution values are maintained constant for 16 hours of the reaction. No other products, such as acetaldehyde, ethylene or acetone have been evidenced for the three catalysts. Although the distribution of the products is congruent between the catalysts, the values of carbon balance are quite different. Indeed, the highest value is registered for the not promoted catalyst. Moreover, the complete carbon balance of 100 % is not achieved. This indicates that a possible reason for the loss of catalytic activity is due to the formation of unwanted carbonaceous species. Therefore, the less active material, the NiZ, has a higher balance of carbon because less products are formed. This point will be widely discussed in the following part of the work. In conclusion, lanthanum addition has strongly affected the catalytic behaviour of NiZ sample nevertheless it didn't affect the distribution of the products. In any case, the synthetic procedure used for lanthanum addition influences the catalytic results.

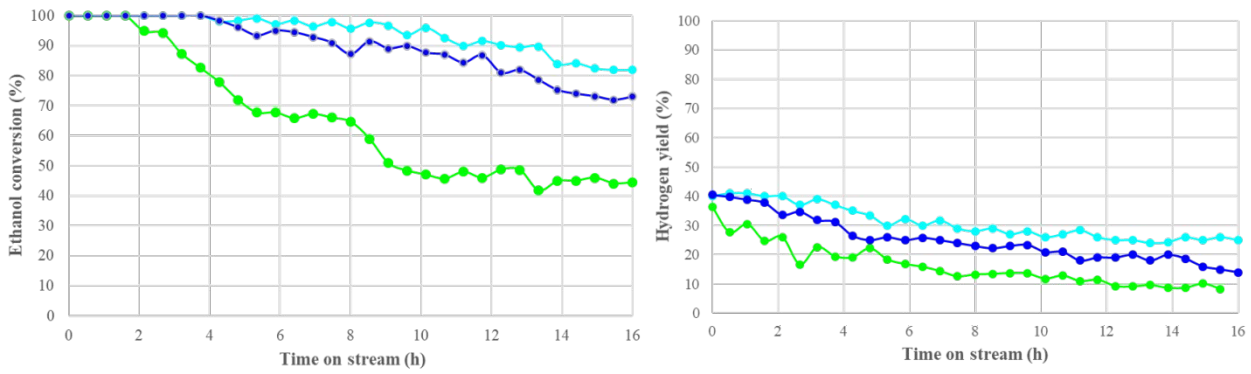

Figure 5: Ethanol conversion (left) and hydrogen yield (right) for NiZ (■), NiLaZ*impr* (▲) and NiLaZ*copr* (●) during test at 550 °C.

	NiZ	**NiLaZ*impr***	**NiLaZ*copr***
H_2 yield (%)	7	25	15
H_2 distribution (%)	74	69	70
CO_2 distribution (%)	25	27	25
CO distribution (%)	1	3	6
EtOH conversion (%)	44	81	73
H_2O Conversion (%)	8	15	20
C Balance (%)	65	55	47

Table 2: Hydrogen yield, products distribution, ethanol and water conversion for NiZ, NiLaZ*impr* and NiLaZ*copr* after 16 hours of reaction at 550 °C.

It is difficult to understand the rapid deactivation of NiZ, as the distribution of the products is the same for all three catalysts. Therefore, to gain insight on the effect of lanthanum, DRIFT-MS analyses were performed only to NiZ and NiLaZr*copr*, since the two promoted samples showed similar catalytic performances.

The infrared spectra with respect to the temperature are reported in the supplementary information (Figure S1 and Figure S2) along with their interpretation.

The spectra of the catalysts recorded in presence of EtOH/H_2O mixture at 500 °C are shown on Figure 6 and Figure 7 for NiZ and NiLaZ*copr*, respectively. It is possible to observe that the base line of the spectra is changing over the time, and this change is different for the two samples. In detail, NiZ base line is not changing over 60 minutes while the NiLaZ*copr* one is dramatically changing. This change can be ascribed to NiO reduction into Ni[40-41]. These results support the H_2-TPR ones, which showed that NiLaZ*copr* possess higher reducibility than NiZ. Remarkably, ethanol/water mixture is not able to completely reduce NiLaZ*copr* in an hour while the same sample when exposed to pure ethanol is

already completely reduced in the very first spectrum at 500 °C, as reported on the right-hand side in Figure S.3. This observation seems to support the idea that ethanol is the reducing agent.

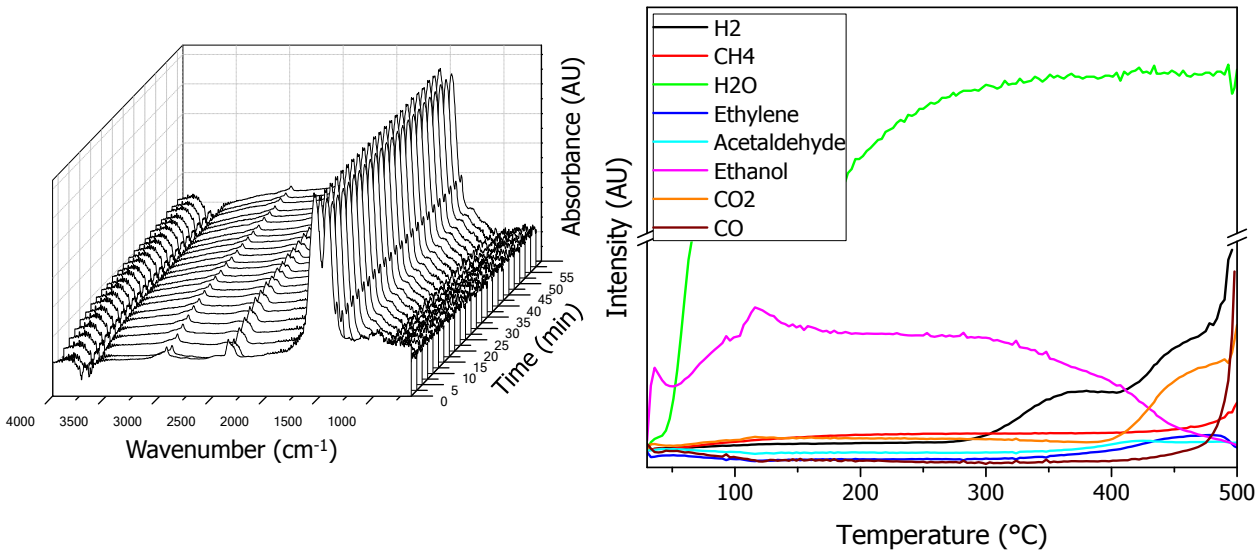

Figure 6 DRIFT spectra recorded at 500 °C and MS spectra from RT to 500 °C feeding EtOH/H_2O on NiZ

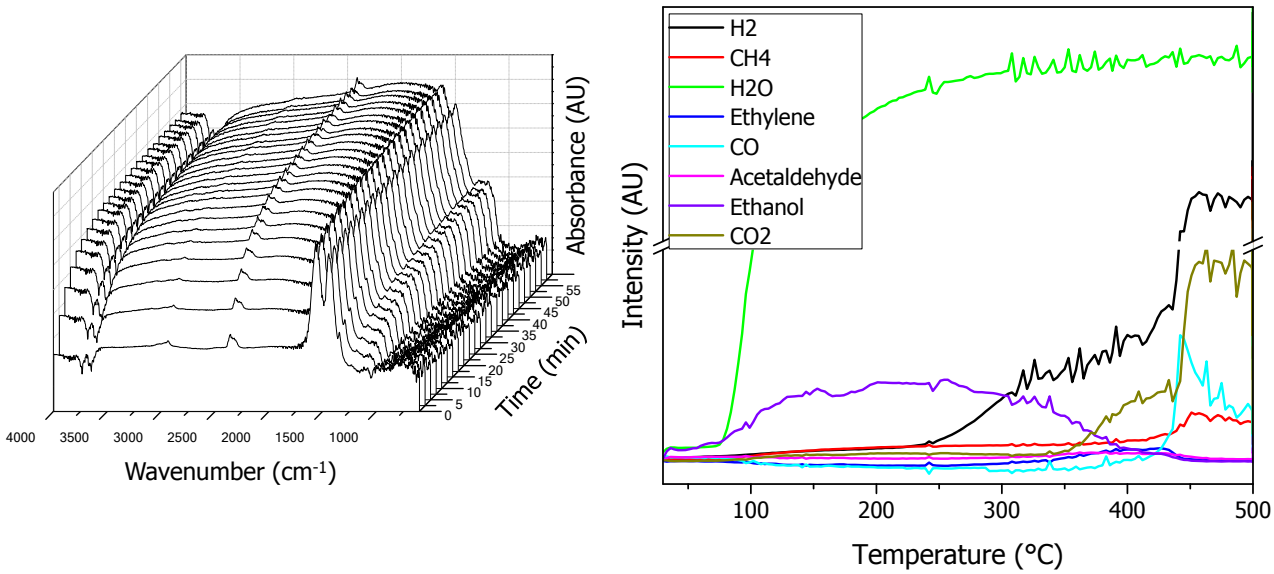

Figure 7 DRIFT spectra recorded at 500 °C and MS spectra from RT to 500 °C feeding EtOH/H_2O on NiLaZ*copr*

The MS ethanol signal increased for both samples until 100 °C, as reported in Figures 6 and 7. All the product signals are strongly influenced by ethanol below 300 °C, and it is not possible to obtain

useful information about their formation. The decreasing profile demonstrated that ethanol started to convert at 300 °C. At the same temperature, acetaldehyde and ethylene intensities increased along with H_2. This is an indication that ethanol dehydration produced ethylene while its oxidative dehydrogenation gave acetaldehyde. In contrast, CO and CO_2 profiles raised at 400 °C. Their formation can be ascribed to acetaldehyde reaction with water:

4) $CH_3CHO + H_2O \rightleftarrows 2\ CO + 3\ H_2$

5) $CH_3CHO + 3\ H_2O \rightleftarrows 5H_2 + 2\ CO_2$

In fact, η^2-acetaldehyde bands were detected on the catalyst surface, as showed in Figure S.2 in the supplementary information. These bands at 400 °C started to decrease supporting the hypothesis of acetaldehyde decomposition reactions. At slightly higher temperature, CH_4 started to be produced probably by acetates transformation to carbonates:

6) $CH_3COO_{(a)} + OH_{(s)} \rightleftarrows CO_{3(a)} + CH_4$

((s) indicates a catalyst moiety; (a) represents an adsorbed specie).

Ethylene and acetaldehyde attained the highest value at 400 °C while CO, CH_4, CO_2 and H_2 profiles came to be sharper. Such an increase is reasonably due to the many reactions of the whole process, such as methanation, WGS and Bouduard, but also to:

7) $CH_3COO_{(a)} + OH_{(s)} \rightleftarrows 2\ CH_4 + CO_{3(a)}$

8) $CH_3COO_{(a)} \rightleftarrows 3/2\ H_2 + 2\ CO_2 + C_{(a)}$

9) $CO_{3(a)} \rightleftarrows CO_2 + O_{(s)}$

10) $CO + O_{(s)} \rightleftarrows CO_2$

The main difference was the ethylene acetaldehyde ratio between the two samples. In fact, NiZ acetaldehyde trend is almost flat suggesting a low production while ethylene trend showed a maximum between 400 °C and 500 °C. In contrast, ethylene and acetaldehyde trends were almost comparable with NiLaZ*copr*. A slight increase in acetaldehyde trend from 300 °C seems to suggest that the oxidative dehydrogenation of ethanol might be favoured with respect to dehydration.

From this analysis it is evident the difference in products distribution between non-promoted and promoted samples even though this difference cannot be depicted during the catalytic tests. The higher production of ethylene for the non-promoted catalyst may be the cause of its deactivation.

In fact, the presence of ethylene can bring to polymerization reaction that lead to coke formation. Acid sites can favour ethylene formation by ethanol dehydration [42]. For this reason, acidic surface analysis was performed using CO_2-TPD technique. In Figure 8 it is reported the CO_2 evolution vs temperature and in Table 3 there are shown the amounts of basic sites obtained by the integration of desorption peaks. In particular, as reported by D. Wierzberg *et al.*[43], three different regions are observed related respectively to basic sites with strong (600-800 °C) medium (300-600 °C) or weak

(50-250 °C) strength. In Table 3 it is also reported the total amount of basic sites. For the promoted sample, such value is an order of magnitude higher than for non promoted one. Knowing that the temperature of the peaks is correlated with the nature of the sites[44], it can be highlighted how the number of medium and strong basic site does the difference. So, the La introduction the support increases boosts the basicity of the support and confines ethanol dehydration, leading to less formation of carbonaceous species consequently. Moreover, basic sites guarantee CO_2 adsorption and disproportion into carbon monoxide and oxygen that could increase the elimination of carbon deposits[45]. For these reasons, both lanthanum doped samples have higher stability and higher hydrogen yield.

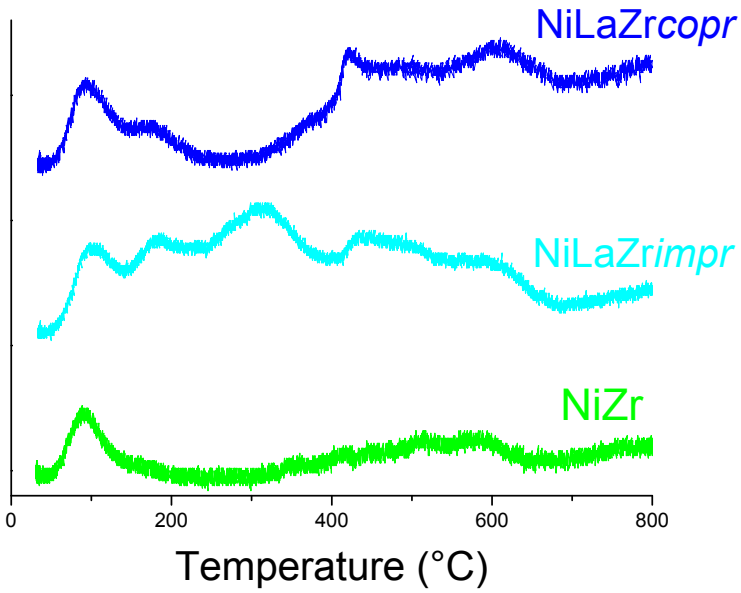

Figure 8: CO_2-TPD of NiZ, NiLaZ*impr* and NiLaZ*copr* catalysts.

	Total basicity (μmol/g)	Weak basic sites (μmol/g)	Medium strength basic sites (μmol/g)	Strong basic sites (μmol/g)
NiZ	108	32	13	63
NiLaZ*impr*	350	114	34	202
NiLaZ*copr*	309	77	63	169

Table 3: Distribution of basic sites for NiZr, NiLaZr*impr* and NiLaZr*copr* samples.

Nevertheless, the different catalytic activity of the promoted samples can also be attributed to the higher basicity of NiLaZ*impr*, which maintains a greater conversion of ethanol and higher hydrogen yield over 16 hours of reaction.

To confirm the promoter effect of lanthanum in avoiding dehydration reaction and understand the differences in its introduction methods, analysation of carbon deposit over the catalytic surface were characterized via SEM, TG and Raman spectroscopy. It is known in literature that deactivation of a sample is mainly ascribable to the nature of formed coke, and not only to its quantity. [46]. As for steam reforming process over nickel, two different kind of coke can be produced: amorphous coke, accountable of the obstruction of metal sites, and filamentous coke, that doesn't affect the metal activity but blocks the entrance of the reagents. Moreover, nature, size, length and thickness of the coke are important parameters that influence the extent of deactivation[47]. The kind of coke depends on the reaction more involved in the process. Montero *et al.* reported that filamentous coke is produced by CH_4 decomposition reaction and Bouduard reaction meanwhile, amorphous coke is produced by ethylene and others oxygenated products condensation[48].

SEM images of used catalysts are showed in Figure 9. Looking at the imagine at low resolution (left), it is evident how filamentous coke is formed in prevalence only in the catalysts NiZ and NiLaZ*copr* while in the catalyst NiLaZ*impr* there is less deposited carbon. This result is confirmed by EDX analysis (Figure 10) in which for NiLaZ*impr*, carbon peak is lower than for the other catalysts. Moreover, regarding the leaching of the active phase, EDX analysis have evidenced that the ratio between the peaks of Ni and Zr has the value of 0.14 for all the catalysts, fresh and used. These data confirm that no loss of active phase was observed.

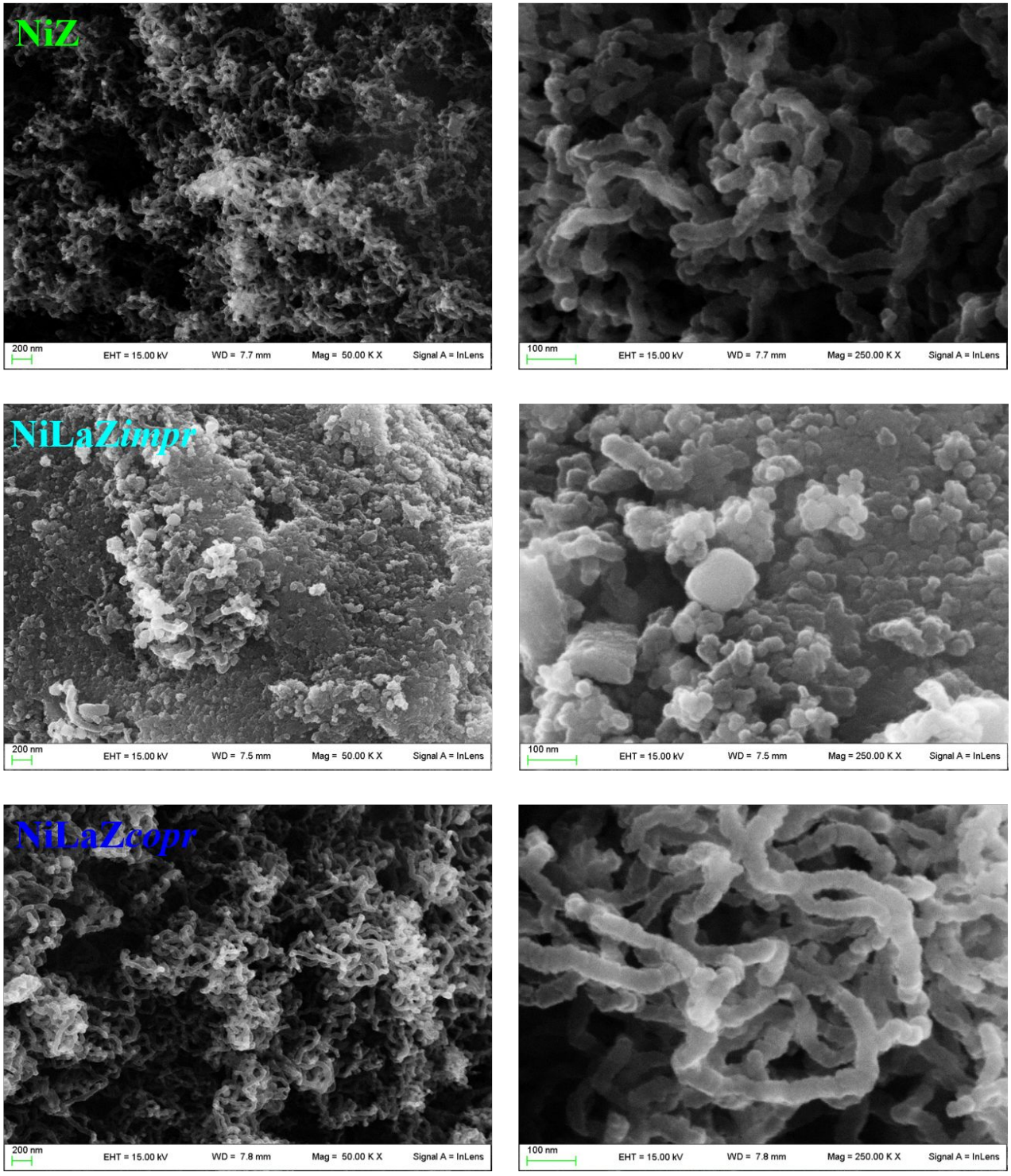

Figure 9: SEM images of NiZ (section a), NiLaZ*impr* (section b) and NiLaZ*copr* (section c) catalysts after ESR test.

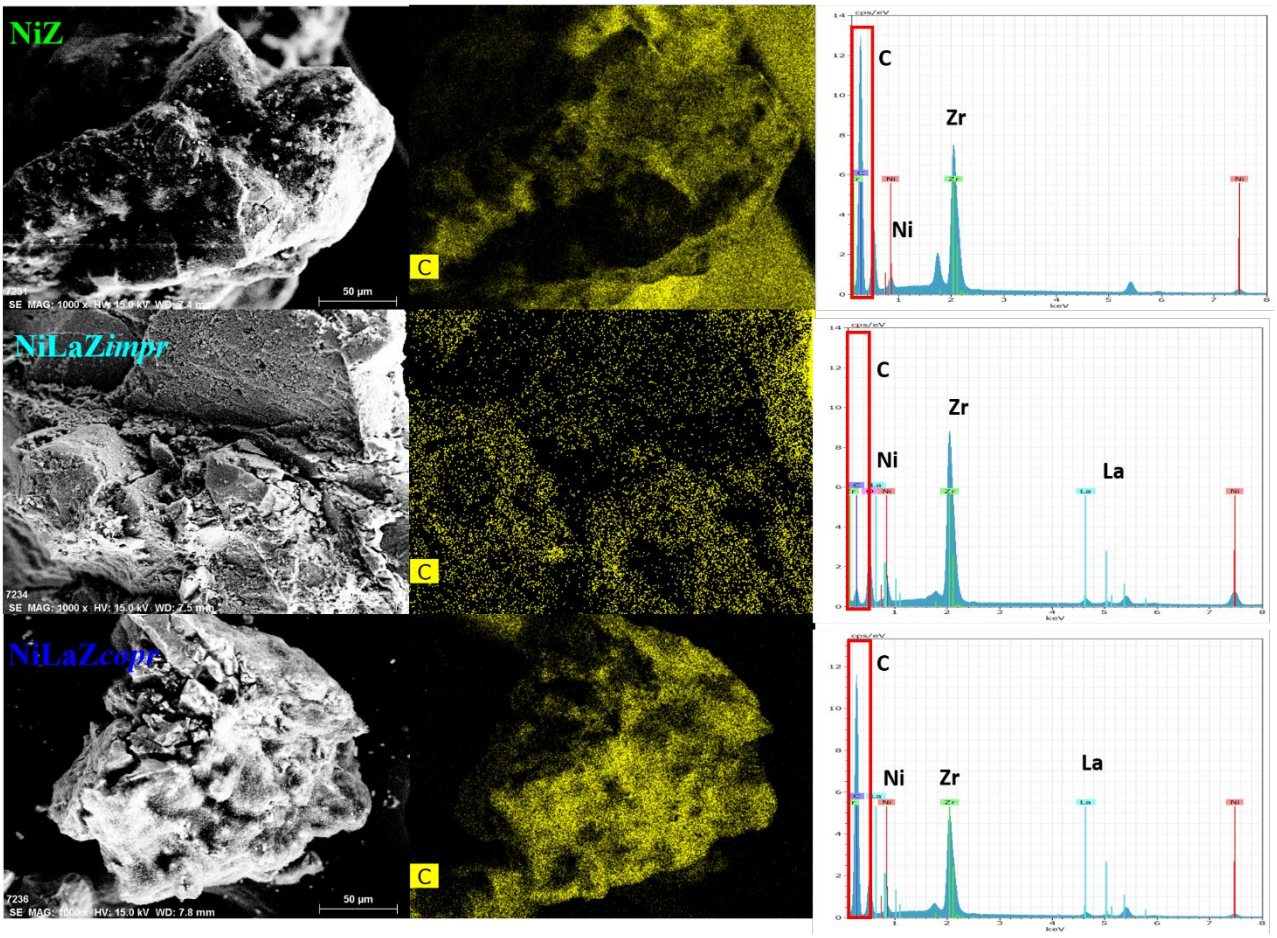

Figure 10: EDX analyses and carbon mapping images of NiZ (section a), NiLaZ*impr* (section b) and NiLaZ*copr* (section c) samples after catalytic test.

To further understand the nature of carbon sediments on the catalysts, Raman spectroscopy was performed[49]. The main features of the spectra (Figure 11) are the Raman bands of carbon structures at about 1350 cm^{-1} and 1600 cm^{-1}, conventionally called D (Defect) and G (Graphite) bands, respectively. The G band is associated with the tangential stretching of C-C bonds with sp^2 hybridization, typical of ordered graphite but also of small sized chains, while D band is associated with the breathing vibrations of carbon atoms rings activated by defects. The presence of a very intense D band and the shift of the G peak from 1580 to 1600 cm^{-1} indicates that for all the samples, the sediments are mainly in the form of nanocrystalline graphite. Multiwall carbon nanotubes (MWCNTs) appear not dominant. In fact, a rough concentration assessment can be obtained from the ratio of the I_D/I_G peaks, assuming a minor contribution of interlayer defects[50-51].

As the I_D/I_G ratio is ~0.8 in NiZ and NiLaZ*copr* samples and ~1 in NiLaZ*imp*, it can be estimated that the MWCNTs concentration is about 20 % in the former samples, while it is below the measurability threshold in NiLa*imp*. Finally, the different morphology of the deposit carbon structures in NiZ samples is further testified by the presence of a small shoulder at 1200 cm^{-1} typical of aliphatic C-H band[40], which is reduced in the co-precipitated sample and practically absent in the impregnated one.

These results prove that, even if coke is produced during the reaction for all the catalysts, lanthanum addition, in particular via impregnation, reduce the formation of aliphatic coke by ethylene polymerization, since it enhances basic properties of the material.

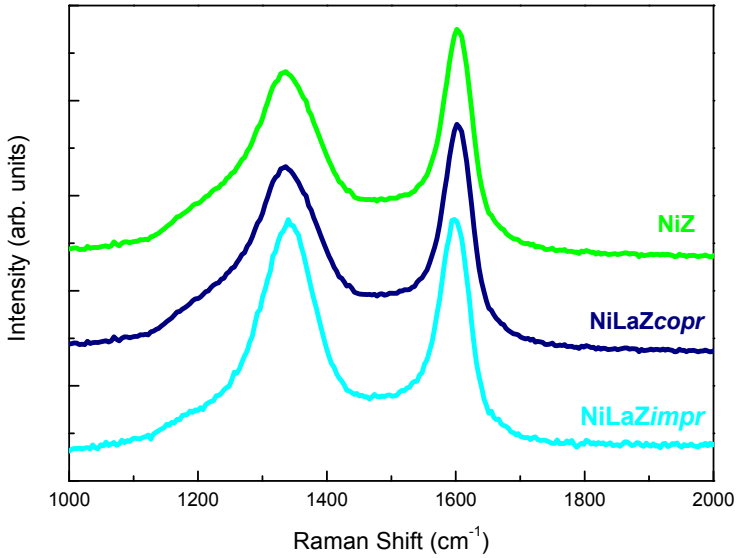

Figure 11: Raman spectroscopy of NiZ, NiLa*Zimpr* and NiLa*Zcopr*.

To properly quantify the amount of carbon deposits over the used catalysts, TG analyses were carried out on NiZ, NiLaZimpr and NiLaZcopr after the catalytic test. In Figure 12, percentage weight loss in function of temperature is represented. In line with other characterizations, not promoted sample shows the highest weight loss of 15 %, meaning the sample has undergone a greater coke coating. This data justifies its faster deactivation. In the case of promoted sample, lower weight loss is visible, 6 wt% for NiLa*Zcopr* and 2 % for NiLa*Zimpr*. Therefore, with this technique a better correlation between the amount of carbon and the stability of the catalyst was obtained. The most active catalyst presents the lowest amount of carbon deposits.

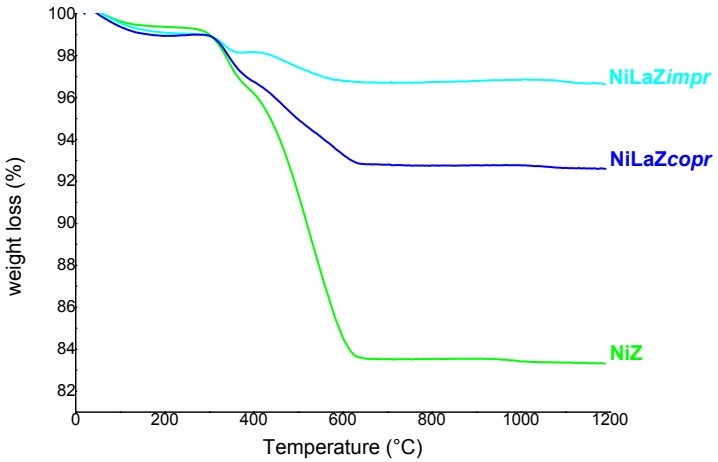

Figure 12: Thermogravimetric analyses of used NiZ, NiLa*Zimpr* and NiLa*Zcopr*

Comparing all the data of hydrogen yield, C balance, carbon deposition and products distribution, a better relationship between the catalytic behavior and the extent of deactivation has been found. NiZ is the less efficient one, since the acidity of the sample is too strong and it facilitates the dehydration reaction, forming carbon nanotubes over the surface and deactivating the catalyst. Indeed, the quantity of coke over the surface is the highest one. Comparing the promoted samples, the impregnated one is the most active material since it shows the majority of medium and strong basic sites. Therefore, its deactivation is slower over time than the other two samples with higher carbon balance and higher hydrogen yield. As for the coprecipitated sample NiLa*Zcopr,* it presents a lower conversion of ethanol than NiLa*Zimpr* with consequently lower hydrogen yield. Indeed, taking into consideration the DRIFT results, the carbon balance, the carbon deposits and the water conversion, NiLa*Zcopr*, after some hours of reaction, prefers the dehydration route than the reforming pathway. As a demonstration of that, the value of water conversion for NiLa*Zcopr* is slightly higher than the value of NiLa*Zimpr*. This work therefore gives, for the first time, a whole representation of how the properties of lanthanum and the way of its addition can vary the single aspects of the zirconia support and the performance of the final catalyst. Zirconia is mainly used as promoter in steam reforming and not as pure support; only few works, as mentioned in the introduction part, reports the combined effect of lanthanum and zirconia as promoter and support for H_2 production by the selected reaction. Moreover, this work has the goal to understand and highlight how the method of promoter's introduction has a strong effect on the morphological and structural properties of the catalyst and as consequence on its catalytic activity. The addition of the promoter by co-precipitation has led to the stabilization of the tetragonal phase of zirconia, despite its low percentage. On the other hand, regarding the catalytic activity, the impregnation method allows the introduction of the appropriate quantity of basic sites of medium and strong strength to suppress the unwanted reactions.

Conclusions

The influence of lanthanum addition on nickel-zirconia catalyst was evaluated. Particularly, lanthanum's effect strongly depends on the introduction method. Addition by incipient wetness impregnation doesn't affect the structural and morphological properties of the material, leaving a similar surface area, pore size distribution and zirconia phases. By contrast, the addition of lanthanum by co-precipitation stabilizes the tetragonal phase of zirconia and increases the surface area of the material. Catalytic performances for ESR were evaluated at 550 °C; improvement in stability and hydrogen distribution for both lanthanum doped catalysts with respect to the not doped catalyst were observed. Not promoted sample is the less efficient one, since the acidity of the sample is too strong and it facilitates the dehydration reaction, forming carbon nanotubes over the surface and deactivating

the catalyst. Indeed, the quantity of coke is the highest one. Comparing the promoted materials, the acidity has been decreased by the addition of lanthanum, as demonstrated by CO_2-TPD analysis. The impregnated sample is the most active material since it shows the majority of medium and strong basic sites. Therefore, its deactivation is slower over time with higher carbon balance and hydrogen yield. In the case of the coprecipitated sample NiLaZ*copr,* it presents a lower conversion of ethanol than NiLaZ*impr* with consequently lower hydrogen yield. Moreover, water conversion of the coprecipitated material is higher than the impregnated one, suggesting that its faster deactivation can be related to the preference of ethanol dehydration route than the reforming pathway after some hours of reactions. Indeed, it presents an higher amount of carbon deposits over its surface as demonstrated by SEM, TG and Raman spectroscopy.

Supporting Information

DRIFTS NiZ feeding EtOH/H_2O continuously as a function of temperature; DRIFTS feeding EtOH-H_2O mixture on NiLaZcopr; DRIFTS at 500 °C feeding EtOH/H_2O and EtOH on NiLaZcopr catalyst

References

1 Liu, Z.; Senanayake, S. D.; Rodriguez, J. A. Catalysts for the Steam Reforming of Ethanol and Other Alcohols, in: Elsevier Inc., Ethanol Science and Engineering, NY, 2019, p.133.

2 Casanovas, A.; Divins, N. J.; Rejas, A.; Bosch R.; Llorca J. Finding a suitable catalyst for on-board ethanol reforming using exhaust heat from an internal combustion engine, *Int. J. Hydrogen Energy* **2017**, *42,* 13681-13690, DOI: 10.1016/j.ijhydene.2016.11.197.

3 Song, J.H.; Han, S.J.; Yoo, J.; Park, S.; Kim, D.H.; Song, I.K. Hydrogen production by steam reforming of ethanol over Ni–X/Al_2O_3–ZrO_2 (X = Mg, Ca, Sr, and Ba) xerogel catalysts: Effect of alkaline earth metal addition, *J. Mol. Catal. Chem.* **2016**, *415,* 151-159, DOI: 10.1016/j.molcata.2016.02.010.

4 Liu, S.; Zhang, K.; Fang, L.; Li, Y. Thermodynamic Analysis of Hydrogen Production from Oxidative Steam Reforming of Ethanol, *Energy Fuels* **2008**, *22,* 1365-1370, DOI: 10.1021/ef700614d.

5 Sharma, Y.C.; Kumar, A.; Prasad, R.; Upadhyay, S. N. Ethanol steam reforming for hydrogen production: Latest and effective catalyst modification strategies to minimize carbonaceous deactivation, *Renewable Sustainable Energy Rev.* **2017**, *74,* 89-103, DOI: 10.1016/j.rser.2017.02.049.

6 Luo, J. Z.; Yu, Z. L.; Ng, C. F.; Au, C. T. CO_2/CH_4 Reforming over Ni–La_2O_3/5A: An Investigation on Carbon Deposition and Reaction Steps, *J. Catal.* **2000**, *194,* 198-210, DOI: 10.1006/jcat.2000.2941.

7 Rossetti, I.; Lassoa, J.; Nichele, V.; Signoretto, M.; Finocchio, E.; Ramis, G.; Di Michele A. Silica and zirconia supported catalysts for the low-temperature ethanol steam reforming, *Appl. Catal., B* **2014**, *150–151,* 257-267, DOI: 10.1016/j.apcatb.2013.12.012.

8 Rossetti, I.; Gallo, A.; Del Santo, V.; Bianchi, C. L.; Nichele, V.; Signoretto, M.; Finocchio, E.; Ramis, G.; Di Michele A. Nickel Catalysts Supported Over TiO_2, SiO_2 and ZrO_2 for the Steam Reforming of Glycerol, *ChemCatChem* **2013**, *5,* 294-306, DOI: 10.1002/cctc.201200481.

9 Nichele, V.; Signoretto, M.; Menegazzo, F.; Gallo, A.; Del Santo, V.; Cruciani, G.; Cerrato, G. Glycerol steam reforming for hydrogen production: Design of Ni supported catalysts, *Appl. Catal., B* **2012** *111–112,* 225-232, DOI: 10.1016/j.apcatb.2011.10.003.

10 Li, D.; Zeng, L.; Li, X.; Wang, X.; Ma, H.; Assabumrungrat, S.; Gong, J. Ceria-promoted Ni/SBA-15 catalysts for ethanol steam reforming with enhanced activity and resistance to deactivation, *Appl. Catal., B* **2015**, *176–177,* 532-541, DOI: 10.1016/j.apcatb.2015.04.020.

11 Osorio-Vargas, P.; Campos, C. H.; Navarro, R. M.; Fierro, J. L.G.; Reyes, P. $Rh/Al_2O_3–La_2O_3$ catalysts promoted with CeO_2 for ethanol steam reforming reaction, *J. Mol. Catal. A: Chem.* **2015**, *407,*169-181, DOI: 10.1016/j.molcata.2015.06.031.

12 Charisiou, N.D.; Papageridis, K.N.; Siakavelas, G.; Sebastian, V.;. Hinder, S.J; Baker, M.A.; Polychronopoulou, K.; Goula, M.A. The influence of SiO_2 doping on the Ni/ZrO_2 supported catalyst for hydrogen production through the glycerol steam reforming reaction, *Catal. Today* **2019**, *319,* 206-219, DOI: 10.1016/j.cattod.2018.04.052.

13 Jung, K. T.; Bell, A. T. The effects of synthesis and pretreatment conditions on the bulk structure and surface properties of zirconia, *J. Mol. Catal. A: Chem.* **2000**, *163,* 27-42, DOI: 10.1016/S1381-1169(00)00397-6.

14 Youn, M.H.; Seo, J.G.; Lee, H.; Bang, Y.; Chung, J.S.; Song, I.K. Hydrogen production by auto-thermal reforming of ethanol over nickel catalysts supported on metal oxides: Effect of support acidity, *Appl. Catal., B* **2010**, *98,* 57-64, DOI: 10.1016/j.apcatb.2010.05.002.

15 Li, W.; Zhao, Z.; Jiao, Y. Dry reforming of methane towards CO-rich hydrogen production over robust supported Ni catalyst on hierarchically structured monoclinic zirconia nanosheets, *Int. J. Hydrogen Energy* **2016**, *41*, 17907-17921, DOI: 10.1016/j.ijhydene.2016.07.272.

16 Ochoa, A.; Aramburu, B.; Ibanez, M.; Valle, B.; Bilbao, J.; Gayubo, A. G.; Castano P., Compositional insights and valorization pathways for carbonaceous material deposited during bio-oil thermal treatment, *ChemSusChem* **2014**, *7,* 2597-2603, DOI: 10.1002/cssc.201402276.

17 Han, S.J.; Bang, Y.; Song, J.H.; Yoo, J.; Park, S.; Kang, K.H; Song, I.K. Hydrogen production by steam reforming of ethanol over dual-templated $Ni–Al_2O_3$ catalyst, *Catal. Today* 2016, *265*, 103-110, DOI: 10.1016/j.cattod.2015.07.041.

18 Song, J. H.; Han, S. J.; Yoo, J.; Park, S.; Kim, D. H.; Song, I. K. Hydrogen production by steam reforming of ethanol over Ni–X/Al_2O_3–ZrO_2 (X = Mg, Ca, Sr, and Ba) xerogel catalysts: Effect of alkaline earth metal addition, *J. Mol. Catal. Chem.* **2016**, *415,* 151-159, DOI: 10.1016/j.molcata.2016.02.010.

19 Nichele, V.; Signoretto, M.; Pinna, F.; Menegazzo, F.; Rossetti, I.; Cruciani, G.; Cerrato, G.; Di Michele A., Ni/ZrO_2 catalysts in ethanol steam reforming: Inhibition of coke formation by CaO-doping, *Appl. Catal., B* **2014**, *150-151,* 12-20, DOI: 10.1016/j.apcatb.2013.11.037.

20 Compagnoni, M.; Tripodi, A.; Di Michele, A.; Sassi, P.; Signoretto, M.; Rossetti, I. Low temperature ethanol steam reforming for process intensification: New Ni/MxO–ZrO_2 active and stable catalysts prepared by flame spray pyrolysis, *Int. J. Hydrogen Energy,* **2017**, *42,* 2819328213, DOI: 10.1016/j.ijhydene.2017.09.123.

21 Campos, C. H.; Osorio-Vargas, P.; Flores-Gonzalez, N. J.; Fierro, L. G.; Reyes, P. Effect of Ni Loading on Lanthanide (La and Ce) Promoted γ-Al_2O_3 Catalysts Applied to Ethanol Steam Reforming, *Catal. Lett.* **2016**, *146,* 433-441, DOI: 10.1007/s10562-015-1649-6.

22 Osorio-Vargas, P.; Campos, C. H.; Navarro, R. M.; Fierro, J. L.G.; Reyes, P. Improved ethanol steam reforming on Rh/Al_2O_3 catalysts doped with CeO_2 or/and La_2O_3: Influence in reaction pathways including coke formation, *Appl. Catal., A,* **2015**, *505,* 159- 172, DOI: 10.1016/j.apcata.2015.07.037.

23 Osorio-Vargas, P.; Flores-González, N. A.; Navarro, R. M.; Fierro, J. L.G.; Campos, C. H.; Reyes, P. Improved stability of Ni/Al_2O_3 catalysts by effect of promoters (La_2O_3, CeO_2) for ethanol steam-reforming reaction, *Catal. Today* **2016**, *259,* 27-38, DOI: 10.1016/j.cattod.2015.04.037.

24 Dan, M.; Mihet, M.; Tasnadi-Asztalos, Z.; Imre-Lucaci, A.; Katona, G.; Laza, M. D. Hydrogen production by ethanol steam reforming on nickel catalysts: Effect of support modification by CeO_2 and La_2O_3, *Fuel* **2015**, *147,* 260-268, DOI: 10.1016/j.fuel.2015.01.050.

25 Bussi, J.; Musso, M.; Veiga, S.; Bespalko, N.; Faccio, R.; Roger, A. Ethanol steam reforming over NiLaZr and NiCuLaZr mixed metal oxide catalysts, *Catal. Today* **2013**, *213,* 42-49, DOI: 10.1016/j.cattod.2013.04.013.

26 Pizzolitto, C.; Menegazzo, F.; Ghedini, E.; Innocenti, G.; Di Michele, A.; Cruciani, G.; Cavani, F.; Signoretto M. Increase of ceria redox ability by lanthanum addition on Ni based catalysts for hydrogen production *ACS SusChemEng* **2018,** *2,* 13867-13876, DOI: 10.1021/acssuschemeng.8b02103.

27 Pizzolitto, C.; Pupulin, E.; Menegazzo, F.; Ghedini, E.; Di Michele, A.; Mattarelli, M.; Cruciani, G.; Signoretto M. Nickel based catalysts for methane dry reforming: Effect of supports on catalytic

activity and stability *Int. J. Hydr. Energy* **2019**, *44 (52),* 28065-28076, DOI: 10.1016/j.ijhydene.2019.09.050.

28 Menegazzo, F.; Manzoli, M.; Di Michele, A.; Ghedini, E.; Signoretto M. Supported Gold Nanoparticles for Furfural Valorization in the Future Bio-based Industry *Topics in Catal.* **2018**, 61 (18-19), 1877-1887, DOI: 10.1007/s11244-018-1003-5.

29 Menegazzo, F.; Pizzolitto, C.; Zanardo, D.; Signoretto, M.; Buysschaert, C.; Beny, G.; Di Michele, A.Hydrogen Production by Ethanol Steam Reforming on Ni-Based Catalysts: Effect of the Support and of CaO and Au Doping *Chemistry Select* **2017**, *2*, 9523-9531, DOI: 10.1002/slct.201702053.

30 Venezia, A. M.; Parola, V. L.; Liotta, L. F. Structural and surface properties of heterogeneous catalysts: Nature of the oxide carrier and supported particle size effects, *Catal. Today* **2017**, *285,* 114-124, DOI: 10.1016/j.cattod.2016.11.004.

31 Molina, R.; Poncelet, G. α-Alumina-Supported Nickel Catalysts Prepared from Nickel Acetylacetonate: A TPR Study, *J. Catal.* **1998**, *173*, 257-267, DOI: 10.1006/jcat.1997.1931.

32 Diskin, A.M.; Cunningham, R.H.; Ormerod, R.M. The oxidative chemistry of methane over supported nickel catalysts, *Catal. Today* **1998**, *46,* 147-154, DOI: 10.1016/S0920-5861(98)00336-8.

33 Nichele, V.; Signoretto, M.; Pinna, F.; Ghedini, E.; Compagnoni, M.; Rossetti, I.; Cruciani, G.; Di Michele A. Bimetallic Ni–Cu Catalysts for the Low-Temperature Ethanol Steam Reforming: Importance of Metal–Support Interactions, *Catal. Lett.* **2015**, *145,* 549-58, DOI: 10.1007/s10562-014-1414-2.

34 Biswas, P.; Kunzru, D. Steam reforming of ethanol for production of hydrogen over Ni/CeO–ZrO catalyst: Effect of support and metal loading, *Int. J. Hydrogen Energy* **2007**, *32,* 969-980, DOI: 10.1016/j.ijhydene.2006.09.031.

35 Nichele, V.; Signoretto, M.; Menegazzo, F.; Rossetti, I.; Cruciani, G. Hydrogen production by ethanol steam reforming: Effect of the synthesis parameters on the activity of Ni/TiO_2 catalysts, *Int. J. Hydrogen Energy* **2014**, *39,* 4252-4258, DOI: 10.1016/j.ijhydene.2013.12.178.

36 Santos, V.; Zeni, M.; Bergmann, C.P.; Hohemberger, J.M. Correlation between thermal treatment and tetragonal/monoclinic nanostructured zirconia powder obtained by sol-gel process, *Rev. Adv. Mater. Sci.* **2008**, *17,* 62-70.

37 Mercera, P.D.L.; van Ommen, J.G.; Doesburg, E.B.M.; Burggraaf, A.J.; Ross, J.R.H. Stabilized tetragonal zirconium oxide as a support for catalysts. Evolution of the texture and structure on calcination in static air, *Appl. Catal.* 1991, *78,* 79-96, DOI: 10.1016/0166-9834(91)80090-J.

38 Li, C.; Li, M. UV Raman spectroscopic study on the phase transformation of ZrO_2, Y_2O_3–ZrO_2 and SO_4^{2-}/ZrO_2, *J. Raman Spectrosc.* **2002**, *33,* 301-308, DOI: 10.1002/jrs.863.

39 Morterra, C.; Cerrato, G.; Pinna, F.; Signoretto, M. Crystal Phase, Spectral Features, and Catalytic Activity of Sulfate-Doped Zirconia Systems, *J. Catal.* 1995, *157,* 109-123, DOI: 10.1006/jcat.1995.1272.

40 Busca, G. Infrared studies of the reactive adsorption of organic molecules over metal oxides and of the mechanisms of their heterogeneously-catalyzed oxidation, *Catal. Today* 1996, *27,* 457-496, DOI: 10.1016/0920-5861(95)00162-X.

41 Busca, G. The use of vibrational spectroscopies in studies of heterogeneous catalysis by metal oxides: an introduction, *Catal. Today* **1996**, *27,* 323-352, DOI: 10.1016/0920-5861(96)88647-0.

42 Rossetti, I.; Biffi, C.; Bianchi, C. L.; Nichele, V.; Signoretto, M.; Menegazzo, F.; Finocchio, E.; Ramis, G.; Di Michele, A. Ni/SiO_2 and Ni/ZrO_2 catalysts for the steam reforming of ethanol, *Appl. Catal., B* **2012**, *117-118*, 384-396, DOI: 10.1016/j.apcatb.2012.02.006.

43 Wierzbickia, D.; Baran, R.; Dębek, R.; Motak, M.; Gálvez, M. E.; Grzybek, T.; Costa, P. D.; Glatzel, P. Examination of the influence of La promotion on Ni state in hydrotalcite-derived catalysts under CO2 methanation reaction conditions: Operando X-ray absorption and emission spectroscopy investigation, *Appl. Catal., B.* **2018**, *232,* 409-419, DOI: 10.1016/j.apcatb.2018.03.089.

44 Zhang, L. ; Wang, X. ; Chen, C.; Zou, X.; Ding, W.; Lu, X. Dry reforming of methane to syngas over lanthanum-modified mesoporous nickel aluminate/γ-alumina nanocomposites by one-pot synthesis, *Int. J. Hydrogen Energy,* 2017, *42,* 11333-11345, DOI: 10.1016/j.ijhydene.2017.03.140.

45 Fan, M.; Abdullah, A. Z.; Bhatia, S. Catalytic Technology for Carbon Dioxide Reforming of Methane to Synthesis Gas, *ChemCatChem* 2009, *1,* 192-208, DOI: 10.1002/cctc.200900025.

46 Bengaard, H. S.; Nørskov, J. K.; Sehested, J.; Clausen, B. S.; Nielsen, L. P.; Molenbroek, A. M.; Rostrup-Nielsen, J. R. Steam Reforming and Graphite Formation on Ni Catalysts, *J. Catal.* **2002,** *209,* 365-384, DOI: 10.1006/jcat.2002.3579.

47 Valle, B.; Aramburu, B.; Benito, P. L.; Bilbao, J.; Gayubo, A. G. Biomass to hydrogen-rich gas via steam reforming of raw bio-oil over Ni/La_2O_3-αAl_2O_3 catalyst: Effect of space-time and steam-to-carbon ratio, *Fuel* **2018**, *216,* 445-455, DOI: 10.1016/j.fuel.2017.11.151.

48 Montero, C.; Ochoa, A.; Castaño, P.; Bilbao, J.; Gayubo, A. G. Monitoring Ni^0 and coke evolution during the deactivation of a Ni/La_2O_3–αAl_2O_3 catalyst in ethanol steam reforming in a fluidized bed, *J. Catal.* **2015**, *331,* 181-192, DOI: 10.1016/j.jcat.2015.08.005.

49 Ferrari A. C.; Robertson, J. Interpretation of Raman spectra of disordered and amorphous carbon, *Phys. Rev. B,* **2000**, *61,*14096, DOI: 10.1103/PhysRevB.61.14095-14107.

50 DiLeo, R. A. Purity assessment of multiwalled carbon nanotubes by Raman spectroscopy, J. *Appl. Phys.* **2007,** *101,* 064307-064311, DOI: 10.1063/1.2712152.

51 Lehman, J.; Terrones, M.; Mansfield, E.; Hurst, K.; Meunier, V. Evaluating the characteristics of multiwall carbon nanotubes, *Carbon* **2011,** *49,* 2581-2602, DOI: 10.1016/j.carbon.2011.03.028.

Table of content (TOC) graphic

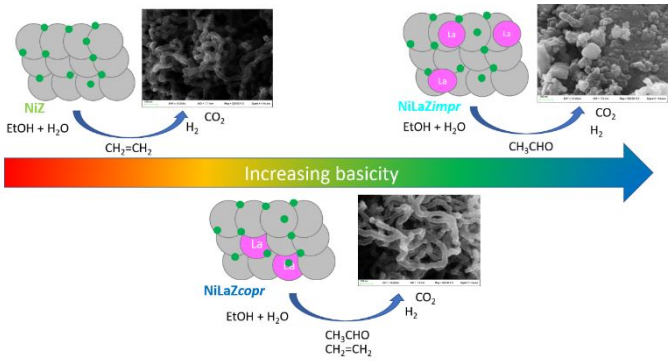

Keywords: zirconia, lanthanum, ethanol steam reforming, coke deactivation

Synopsis: The synthetic methodology of lanthanum addition on Ni/ZrO_2 strongly affected its properties and performances in ethanol steam reforming.